active X chromosome, was shown to be reactivated after transfer into an enucleated oocyte, but then became preferentially inactivated in extraembryonic tissues. In light of the results we present here, these findings are consistent with the idea that the presence of a transcribing *Xist* gene, whether paternally inherited or of somatic cell origin, is likely to be the only "imprint" required to trigger the chromatin modifications and epigenetic marks that lead to preferential X inactivation in the cleavage stage embryo.

References and Notes

1. M. F. Lyon, *Nature* **190**, 372 (1961).
2. M. Monk, *Cytogenet. Genome Res.* **99**, 200 (2002).
3. N. Takagi, M. Sasaki, *Nature* **256**, 640 (1975).
4. J. D. West, W. I. Frels, V. M. Chapman, V. E. Papaioannou, *Cell* **12**, 873 (1977).
5. M. F. Lyon, S. Rastan, *Differentiation* **26**, 63 (1984).
6. S. Rastan, *J. Embryol. Exp. Morphol.* **41**, 11 (1982).
7. N. Takagi, O. Sugawara, M. Sasaki, *Chromosoma* **85**, 275 (1982).
8. G. D. Penny, G. F. Kay, S. A. Sheardown, S. Rastan, N, Brockdorff, *Nature* **379**, 131 (1996).
9. Y. Marahrens, B. Panning, J. Dausman, W. Strauss, R. Jaenisch, *Genes Dev.* **11**, 156 (1997).
10. A. Wutz, R. Jaenisch, *Mol. Cell.* **5**, 695 (2000).
11. G. F. Kay, S. C. Barton, M. A. Surani, S. Rastan, *Cell* **77**, 639 (1994).
12. T. B. Nesterova, S. C. Barton, M. A. Surani, N, Brockdorff, *Dev. Biol.* **235**, 343 (2001).
13. M. Zuccotti *et al.*, *Mol. Reprod. Dev.* **61**, 14 (2002).
14. N. Takagi, *Exp. Cell. Res.* **86**, 127 (1974).
15. O. Sugawara, N. Takagi, M. Sasaki, *Cytogenet. Cell Genet.* **39**, 210 (1985).
16. C. J. Epstein, S. Smith, B. Travis, G. Tucker, *Nature* **274**, 500 (1978).
17. P. G. Kratzer, S. M. Gartler, *Nature* **274**, 503 (1978).
18. M. Monk, M. I. Harper, *Nature* **281**, 311 (1979).
19. J. Singer-Sam, V. M. Chapman, J. M. Lebon, A. D. Riggs, *Proc. Natl. Acad. Sci. U.S.A.* **89**, 10469 (1992).
20. K. E. Latham, L. Rambhatla, *Dev. Genet.* **17,** 212 (1995).
21. M. Monk, A. McLaren, *J. Embryol. Exp. Morphol.* **63**, 75 (1981).
22. I. Okamoto, S. S. Tan, N. Takagi, *Development* **127**, 4137 (2000).
23. J. Matsui, Y. Goto, N. Takagi, *Hum. Mol. Genet.* **10**, 1393 (2001).
24. E. Heard *et al.*, *Cell* **107**, 727 (2001).
25. W. Mak *et al.*, *Curr. Biol.* **12**, 1016 (2002).
26. J. Silva *et al.*, *Dev. Cell.* **4**, 481 (2003).
27. K. Plath *et al.*, *Science* **300,** 131 (2003).
28. A. H. Peters *et al.*, *Cell* **107**, 323 (2001).
29. C. Costanzi *et al.*, *Development* **127**, 2283 (2000).
30. J. Chaumeil, I. Okamoto, M. Guggiari, E. Heard, *Cytogenet. Genome Res.* **99**, 75 (2002).
31. J. M. Lebon *et al.*, *Genet. Res.* **65**, 223 (1995).
32. A. K. Hadjantonakis, L. L. Cox, P. P. Tam, A. Nagy, *Genesis* **29**, 133 (2001).
33. M. Patturajan *et al.*, *Mol. Cell. Biol.* **18**, 2406 (1998).
34. J. Chaumeil, E. Heard, in preparation.
35. I. Okamoto, A. P. Otte, C. D. Allis, D. Reinberg, E. Heard, data not shown.
36. J. Rossant, *J. Embryol. Exp. Morphol.* **33**, 991 (1975).
37. See A. P. Otte, T. H. Kwaks, *Curr. Opin. Genet. Dev.* **13**, 448 (2003) for a review.
38. V. E. Papaiioannou, J. D. West, *Genet. Res.* **37**,183 (1981).
39. J. B. Gurdon, J. A. Byrne, S, Simonsson, *Proc. Natl. Acad. Sci. U.S.A.* **100**, 11819 (2003).
40. T. Moore *et al.*, *Dev. Genet.* **17**, 206 (1995).
41. K. Eggan *et al.*, *Science* **290**, 1578 (2000).
42. Materials and methods are available as supporting material on *Science* Online.

43. We thank N. Takagi, V. Colot, and J. Chaumeil for critical reading of the manuscript; J. B. Sibarita for help with 3D microscopy; and S. Yoshida for her encouragement. I.O. was supported by the Japanese Society for the Promotion of Science. This work was funded by the CNRS, the Association pour la Recherche sur le Cancer, and the Fondation pour la Recherche Medicale.

Supporting Online Material
www.sciencemag.org/cgi/content/full/1092727/DC1
Materials and Methods
Figs. S1 to S4
Table S1
References and Notes

20 October 2003; accepted 1 December 2003
Published online 11 December 2003;
10.1126/science.1092727
Include this information when citing this paper.

REPORTS

Extinct Technetium in Silicon Carbide Stardust Grains: Implications for Stellar Nucleosynthesis

Michael R. Savina,[1]* Andrew M. Davis,[2,3] C. Emil Tripa,[1,2] Michael J. Pellin,[1] Roberto Gallino,[4] Roy S. Lewis,[2] Sachiko Amari[5]

The isotopic composition of ruthenium (Ru) in individual presolar silicon carbide (SiC) stardust grains bears the signature of *s*-process nucleosynthesis in asymptotic giant branch stars, plus an anomaly in ^{99}Ru that is explained by the in situ decay of technetium isotope ^{99}Tc in the grains. This finding, coupled with the observation of Tc spectral lines in certain stars, shows that the majority of presolar SiC grains come from low-mass asymptotic giant branch stars, and that the amount of ^{99}Tc produced in such stars is insufficient to have left a detectable ^{99}Ru anomaly in early solar system materials.

Presolar grains, remnants of stars that lived and died before the solar system formed, have much to teach us about stellar evolution and nucleosynthesis. Most of the grains initially present in the protosolar nebula were melted or vaporized when the solar system formed, and were transformed into new mineral phases with isotopic compositions representing an average over all the material present. Some grains, however, accreted into protoplanetary bodies that did not experience substantial heating, survived low-temperature aqueous alteration in those bodies, and are found today in primitive meteorites (*1*, *2*). Each of these presolar grains carries an isotopic record of the initial composition and nuclear processing in its parent star. Silicon carbide grains are the best studied because of their relatively large size (up to several micrometers) and relatively high abundance (up to a few tens of ppm in primitive meteorites) (*3*). Their heavy element concentrations are high enough (up to a few tens of ppm) (*4*) to permit isotopic analysis of trace elements in individual grains. The majority (>90%) of SiC grains were produced in late stellar outflows of low mass (~1.5 to 3 $M_{\odot}$, where $M_{\odot}$ is the mass of the Sun) asymptotic giant branch (AGB) stars (*5*). In AGB stars, elements heavier than Fe are synthesized quiescently by slow neutron capture (the *s*-process), while in massive stars (≥10 $M_{\odot}$) heavy elements are synthesized under explosive conditions by rapid neutron capture (the *r*-process) or by proton capture/photodisintegration reactions (the *p*-process) (*6*). The isotopic compositions of Zr (*7*), Mo (*8*), Sr (*9*), and Ba (*10*) in mainstream SiC grains show the *s*-process signatures predicted by models of nucleosynthesis in carbon-rich low-mass AGB stars from which SiC can condense (*11*).

The pioneering observation of Tc (half-life $T_{1/2} = 2.1 \times 10^5$ years) in the spectra of certain red giants (later recognized as AGB stars) by Merrill more than 50 years ago (*12*) proved that *s*-process nucleosynthesis is ongoing in those stars. Technetium has since been detected in a large proportion of MS, S, and C stars (red giants at various stages of evolution along the AGB) (*13*, *14*). ^{99}Tc lies along the *s*-process path (Fig. 1) and is the only abundant Tc isotope produced in low-mass AGB stars. The

[1]Materials Science Division, Argonne National Laboratory, Argonne, IL 60439, USA. [2]Enrico Fermi Institute, [3]Department of the Geophysical Sciences, University of Chicago, Chicago, IL 60637, USA. [4]Dipartimento di Fisica Generale, Università di Torino and Sezione INFN di Torino, I-10125 Torino, Italy. [5]Laboratory for Space Sciences and Department of Physics, Washington University, St. Louis, MO 63130, USA.

*To whom correspondence should be addressed. E-mail: msavina@anl.gov

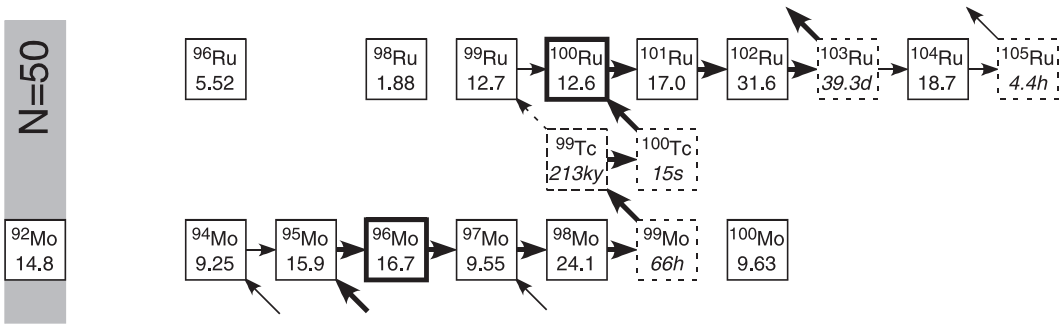

Fig. 1. Chart of the nuclides in the Ru region. Percent abundances (nonitalic) are shown for each stable isotope; laboratory half-lives (italic) are shown for each unstable isotope. The main *s*-process path is shown as bold arrows, and branches along the *s*-path are shown as finer arrows; ^{99}Tc decay that occurs in the envelope after TDU is shown as a dashed arrowtail. Unstable nuclei are outlined in dashed lines; *s*-process–only isotopes are outlined in bold. ^{96}Ru and ^{98}Ru are *p*-process isotopes; ^{100}Ru is an *s*-process–only isotope (it is shielded from the *r*-process by stable ^{100}Mo); ^{104}Ru is an *r*-process isotope; and ^{99}Ru,^{101}Ru, and ^{102}Ru are produced by both the *r*- and *s*-processes.

^{99}Tc/^{99}Ru decay couple has been investigated as a means of discovering the time scales of early solar system processes such as planetary differentiation and the injection of *s*-process material into the protosolar nebula. However, studies of the Ru/Tc isotopic composition in nonpresolar meteoritic materials have found very small (generally less than 1 part per 10,000) deviations, or none at all, relative to average solar system material (*15*–*18*). In contrast, presolar grains present an opportunity to study Ru in materials in which isotopic anomalies should be large [per mil (‰) in the hundreds], because the grains are unaffected by mixing processes in the protosolar nebula.

The *s*-process in AGB stars produces Ru and Tc isotopes with a distinct isotopic signature. Because the half-life of ^{99}Tc is comparable to the period over which the star is nucleosynthetically active, live ^{99}Tc should be present in the stellar winds from which SiC grains condense. Daughters of other now-extinct short-lived nuclides have been detected in presolar grains. For example, ^{26}Al ($T_{1/2}$ = 7.1×10^5 years) gives rise to excess ^{26}Mg in presolar SiC (*19*). Conversely, the nondetection of excess ^{135}Ba, the daughter of *s*-process ^{135}Cs ($T_{1/2} = 6.3 \times 10^6$ years), has been attributed to the high volatility of Cs preventing its condensation in SiC grains (*11*). Therefore, the study of Ru isotopes in grains provides a test of stellar nucleosynthesis models and a baseline for future searches for extinct ^{99}Tc in solar system materials.

Forty grains isolated from the Murchison meteorite (fraction KJG, mount CHRL108, average grain size 3 μm) (*20*) were analyzed by resonant ionization mass spectrometry (*21*, *22*). Isobaric interferences believed to be due to the major isotopomers of Si_3C compromised the data for the *p*-process isotopes ^{96}Ru and ^{98}Ru in most grains, but the remaining Ru isotopes were free of interferences. Twenty-one of the 40 grains had detectable amounts of Ru. Among these 21 grains, 19 had the distinctive *s*-process Ru isotopic composition (table S1), whereas two had *r*-process enhancements and are thus not mainstream SiC. Of the 19 grains with *s*-process Ru, two were known from previous C, N, and Si isotopic analysis to be mainstream SiC.

The *r*- and *p*-process contributions found in solar system Ru are low in these grains. Normalized to the *s*-process–only ^{100}Ru, the *p*-process isotopes ^{96}Ru and ^{98}Ru and the *r*-process isotope ^{104}Ru show strong depletions, whereas smaller depletions are seen in the partially *s*-process isotopes ^{99}Ru, ^{101}Ru, and ^{102}Ru (Fig. 2). This is the *s*-process signature expected from low-mass AGB stars and results from the strong production of ^{100}Ru relative to the lesser production and even slight consumption (~2% for ^{96}Ru and ^{98}Ru) of the other isotopes.

A low-mass AGB star is composed of an inert carbon-oxygen core and a H-rich envelope, separated by a He-rich intershell. A tiny region enriched in ^{13}C (the ^{13}C pocket) forms in the top layers of the intershell and provides a steady low-flux neutron exposure via the ^{13}C(α,*n*)^{16}O reaction. Hydrogen burning at the base of the envelope normally powers the star; however, thermal pulses caused by periodic quasi-explosive He-burning induces mixing of a small amount of He intershell material into the convective envelope in so-called third dredge-up (TDU) episodes. A low-mass star undergoes a few tens of thermal pulses as the star evolves, and material dredged up from the He intershell enriches the envelope in ^{12}C and *s*-process products. Late in the AGB phase, when the envelope C/O ratio exceeds 1, graphite and carbides such as SiC condense as strong stellar winds remove matter from the envelope. The star loses mass from the envelope at an increasing rate until finally ejecting the remainder of its envelope after the last thermal pulse, which terminates the AGB phase and leaves behind a nascent white dwarf.

Nucleosynthesis models for AGB stars were computed using the FRANEC stellar evolution code and the Torino *s*-process post-processing code (*11*, *23*). Models were computed for 1.5 $M_\odot$ and 3 $M_\odot$ stars, but there was no significant difference in the Ru predictions and we discuss only the 1.5 $M_\odot$ models here. The models assume initially solar metallicity and isotopic composition, although a range of metallicities was explored. The amount of ^{13}C in the He intershell is a free parameter. The "standard case" has a ^{13}C pocket that, for stars with half of the solar metallicity, reproduces the main *s*-process component in the solar system (i.e., *s*-process nuclei from Zr to Pb) (*24*). Models were computed for eight ^{13}C pocket sizes. The smallest pocket had almost no ^{13}C, whereas the largest had twice the amount of the standard case. Larger pockets are implausible because ingesting more protons into the intershell only drives proton capture on ^{13}C to produce ^{14}N. The 1.5 $M_\odot$ model experiences 17 TDU episodes and has C/O > 1 for the last nine thermal pulses. Uncertainties in the model predictions due to the choice of neutron capture cross sections were calculated by varying the cross sections for ^{99}Ru, ^{101}Ru, ^{102}Ru, and ^{99}Tc within the error limits of the measurements (*25*).

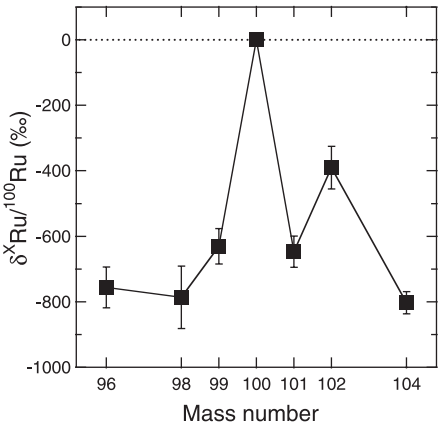

Fig. 2. Ru isotopic pattern of a known mainstream SiC grain (CHRL108 326-3) showing the large deviations from terrestrial Ru characteristic of the *s*-process. The grain data were indexed to the *s*-only isotope ^{100}Ru and normalized to the isotopic composition measured in a Ru single crystal standard according to $\delta^x\text{Ru}$ (‰) = $1000 \times [(^x\text{Ru}/^{100}\text{Ru})_{\text{grain}} / (^x\text{Ru}/^{100}\text{Ru})_{\text{standard}} - 1]$ (i.e., parts per thousand deviation from solar system Ru). Although many grains have isobaric interferences at ^{96}Ru and ^{98}Ru, this grain apparently does not, so the full pattern is shown. The error bars are 2σ.

The measured and predicted values for ^{101}Ru agree, whereas the measured ^{99}Ru and ^{102}Ru deviate from the predictions (Fig. 3). In

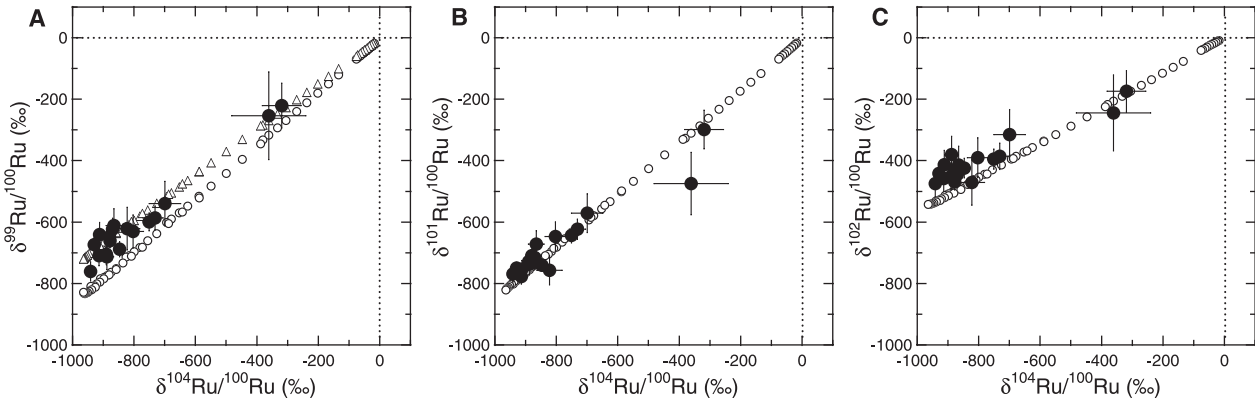

Fig. 3. (**A**) δ^{99}Ru, (**B**) δ^{101}Ru, and (**C**) δ^{102}Ru versus δ^{104}Ru comparing presolar SiC grain data (solid circles) with predictions for 1.5 $M_{\odot}$ AGB stars (open circles). Uncertainties on the measured points are 2σ. Model predictions for each ^{13}C pocket are plotted only for conditions under which SiC can condense (i.e., when the C/O ratio in the stellar envelope is >1). Predicted points lie near the origin for small ^{13}C pockets and become increasingly negative as the ^{13}C pockets increase in size. The δ^{99}Ru plot (A) also shows the values predicted by including in situ decay of ^{99}Tc in grains, assuming a Tc:Ru condensation ratio of 1:1 (triangles).

Table 1. Comparison of Ru G-components in SiC mainstream grains with those predicted for 1.5 $M_{\odot}$ AGB stars. Uncertainties are 2σ. For the grain data, uncertainties are determined by counting statistics and scatter about the regression lines (*32*); the uncertainties in the calculations are determined by uncertainties in the neutron capture cross sections.

Isotope	Deviation from solar value (‰)		
	Measured G-component	Calculated G-component	Calculated ^{99}Ru + ^{99}Tc G-component
^{99}Ru	−755 ± 11	−839 ± 17	−734 ± 30
^{101}Ru	−825 ± 10	−839 ± 14	
^{102}Ru	−495 ± 13	−554 ± 55	

the case of ^{102}Ru (Fig. 3C), the discrepancy is within the range allowed by the present uncertainties in the neutron capture cross sections, but the measured δ^{99}Ru values (Fig. 3A) lie outside the uncertainties in predictions. If, however, we assume that live ^{99}Tc condensed into the grains at the same Tc/Ru ratio as in the envelopes of the parent stars (~1/3), the data and predictions agree.

Linear fits to the grain data, weighted by the uncertainties in the δ values, represent mixing lines between the initial stellar composition (the "N-component") and an *s*-process composition (the "G-component"). In our model, the G-component corresponds to the average isotopic composition of all the Ru produced in the He intershell and dredged up into the envelope over the history of the AGB phase of the star. The regressions were constrained to pass through solar composition and represent mixing lines between a solar N-component [(δ^{104}Ru, δ^{x}Ru) ≡ (0, 0)] and the calculated G-component at δ^{104}Ru = –987‰ (*26*). Measured and calculated G-components for ^{101}Ru and ^{102}Ru agree at the 2σ level when uncertainties in the neutron capture cross sections are taken into account (Table 1).

Presolar grain data such as these can be used to better constrain neutron capture cross sections (*27*). Our model reproduces the measured ^{102}Ru G-component if the ^{102}Ru neutron capture cross section is decreased by 10% (present 2σ uncertainty = 12%). The same is true if the ^{100}Ru cross section is increased by 5% (2σ uncertainty = 12%) while the ^{102}Ru cross section is decreased by 5%. Neither of these scenarios affects the G-components of the other isotopes by amounts measurable by our technique.

For ^{99}Ru, we observe a G-component 84‰ higher than the calculated one and far outside the 2σ limits. The calculated ^{99}Ru G-component is robust given the uncertainties in the cross sections of ^{99}Tc (2σ = 6%) and ^{100}Ru; the value varies by only 17‰ when these uncertainties are taken into account. The ^{99}Ru G-component obtained by summing the ^{99}Tc and ^{99}Ru produced in the model, which is the value we expect if SiC grains condense with the Ru/Tc ratio of the envelope and Tc subsequently decays to Ru, is consistent with our measured value.

Even at the temperatures reached in the ^{13}C pocket, the half-life of ^{99}Tc is long compared to the few tens of thousands of years between TDU episodes (*28*). Therefore, ^{99}Tc behaves like a stable *s*-process isotope while the ^{13}C pocket is active. In contrast, ^{99}Ru behaves like the *p*-isotopes ^{96}Ru and ^{98}Ru; all of the ^{99}Ru that passes through the ^{13}C pocket (~2% of the initial amount in the star) is consumed by neutron capture. Therefore, all of the ^{99}Ru produced by AGB stars is radiogenic from ^{99}Tc. Some ^{99}Tc decays in the stellar envelope, but some survives the AGB phase. The mass 99 budget in newly formed grains therefore comprises residual unprocessed ^{99}Ru, daughter ^{99}Ru from ^{99}Tc decay in the stellar envelope, and live ^{99}Tc. It is this last material that we detect as excess δ^{99}Ru relative to the model prediction.

The calculated 50% condensation temperatures of Tc and Ru in metallic solid solution are within 20 K of each other under conditions appropriate for the protosolar nebula (*29*). However, Ru and Tc condensed into SiC in the circumstellar envelopes of AGB stars, either as carbides or as metal grains that were later trapped in SiC. X-ray fluorescence studies show that the Ru/Mo ratio in presolar SiC grains matches the predictions for 1.5 $M_{\odot}$ and 3 $M_{\odot}$ stars at the end of the AGB stage (*30*). Molybdenum is believed to condense as a carbide, so it seems likely that Ru and Tc condense as carbides also. These elements are refractory enough that they either condense before SiC or in solid solution in the first few percent of SiC condensation. Thus, we expect that Tc should condense into mainstream SiC grains at a Tc/Ru ratio matching that of the stellar envelope, which is consistent with our measurements.

Small deviations in the bulk Ru isotopic composition of differentiated meteorites could be interpreted as evidence of live ^{99}Tc in the early solar system if one assumes mixing of freshly minted AGB material with the protosolar nebula just before (and perhaps triggering) its collapse. Our measurements of the amount of ^{99}Tc produced in AGB stars confirm that even under the assumption that the mixing and collapse were instantaneous, ^{99}Ru deviations due to in situ ^{99}Tc decay in meteoritic materials would be less than about 3 parts per 100,000 (*31*), which is comparable to the precision limit of current measurements (*17*, *18*). The likelihood of finding

evidence for live ^{99}Tc in the early solar system is therefore small.

References and Notes

1. R. S. Lewis, M. Tang, J. F. Wacker, E. Anders, E. Steel, *Nature* **326**, 160 (1987).
2. T. Bernatowicz *et al*., *Nature* **330**, 728 (1987).
3. E. Zinner, *Meteorit. Planet. Sci.* **33**, 549 (1998).
4. S. Amari, P. Hoppe, E. Zinner, R. S. Lewis, *Meteoritics* **30**, 679 (1995).
5. P. Hoppe, U. Ott, in *Astrophysical Implications of the Laboratory Study of Presolar Materials,* T. J. Bernatowicz, E. Zinner, Eds. (American Institute of Physics, Woodbury, NY, 1996), pp. 27–58.
6. B. S. Meyer, *Annu. Rev. Astron. Astrophys.* **32**, 153 (1994).
7. G. K. Nicolussi *et al*., *Science* **277**, 1281 (1997).
8. G. K. Nicolussi *et al*., *Geochim. Cosmochim. Acta* **62**, 1093 (1998).
9. G. K. Nicolussi *et al*., *Phys. Rev. Lett.* **81**, 3583 (1998).
10. M. R. Savina *et al*., *Geochim. Cosmochim. Acta* **67**, 3201 (2003).
11. M. Lugaro *et al*., *Astrophys. J.* **593**, 486 (2003).
12. P. W. Merrill, *Astrophys. J.* **116**, 21 (1952).
13. S. J. Little, I. R. Little-Marenin, W. H. Bauer, *Astron. J.* **94**, 981 (1987).
14. V. V. Smith, D. L. Lambert, *Astrophys. J.* **311**, 843 (1986).
15. H. Poths, S. Schmitt-Strecker, F. Begemann, *Geochim. Cosmochim. Acta* **51**, 1143 (1987).
16. I. D. Hutcheon, J. T. Armstrong, G. J. Wasserburg, *Geochim. Cosmochim. Acta* **51**, 3175 (1987).
17. H. Becker, R. J. Walker, *Chem. Geol.* **196**, 43 (2003).
18. J. H. Chen, D. A. Papanastassiou, G. J. Wasserburg, *Lunar Planet. Sci.* **XXXIV**, 1789 (2003).
19. P. Hoppe, S. Amari, E. Zinner, T. Ireland, R. S. Lewis, *Astrophys. J.* **430**, 870 (1994).
20. S. Amari, R. S. Lewis, E. Anders, *Geochim. Cosmochim. Acta* **58**, 459 (1994).
21. Z. Ma, R. N. Thompson, K. R. Lykke, M. J. Pellin, A. M. Davis, *Rev. Sci. Instrum.* **66**, 3168 (1995).
22. M. R. Savina *et al*., *Geochim. Cosmochim. Acta* **67**, 3215 (2003).
23. R. Gallino *et al*., *Astrophys. J.* **497**, 388 (1998).
24. C. Arlandini *et al*., *Astrophys. J.* **525**, 886 (1999).
25. Z. Y. Bao *et al*., *Atom. Data Nucl. Data Tables* **76**, 70 (2000).
26. In our model, each ^{13}C pocket gives rise to a unique G-component; however, they are all the same within 5‰, so we compare our data to the average. The Ru G-component is not at δ^{104}Ru = –1000‰, corresponding to no ^{104}Ru at all, because a small amount of ^{104}Ru is produced by bridging ^{103}Ru, whose 39-day half-life is long enough to permit a few captures during the *s*-process neutron exposure (see Fig. 1).
27. F. Voss, K. Wisshak, K. Guber, F. Käppeler, G. Reffo, *Phys. Rev. C* **50**, 2582 (1994).
28. K. Takahashi, K. Yokoi, *Atom. Data Nucl. Data Tables* **36**, 375 (1987).
29. B. Fegley, K. Lodders, H. Palme, *Meteoritics* **28**, 346 (1993).
30. Y. Kashiv, personal communication.
31. G. J. Wasserburg, M. Busso, R. Gallino, C. M. Raiteri, *Astrophys. J.* **424**, 412 (1994).
32. J. H. Williamson, *Can. J. Phys.* **46**, 1845 (1968).

33. We thank R. N. Clayton, L. Nittler, and two anonymous reviewers for careful reading of this paper. Supported by the U.S. Department of Energy, Basic Energy Sciences–Material Sciences under contract W-31-109-ENG-38; NASA grants 8336 (S.A.), 9510 (A.M.D.), and an unnumbered grant (M.J.P.); the University of Chicago; and the Italian FIRB Progetto Origine Astrofisica degli Elementi Pesanti Oltre il Ferro. The University of Chicago operates Argonne National Laboratory under contract with the U.S. Department of Energy.

Supporting Online Material

www.sciencemag.org/cgi/content/full/303/5658/649/DC1
Table S1

28 July 2003; accepted 2 December 2003

Elastic Torque and the Levitation of Metal Wires by a Nematic Liquid Crystal

C. Lapointe, A. Hultgren, D. M. Silevitch, E. J. Felton, D. H. Reich, R. L. Leheny

Anisotropic particles suspended in a nematic liquid crystal disturb the alignment of the liquid crystal molecules and experience small forces that depend on the particles' orientation. We have measured these forces using magnetic nanowires. The torque on a wire and its orientation-dependent repulsion from a flat surface are quantitatively consistent with theoretical predictions based on the elastic properties of the liquid crystal. These forces can also be used to manipulate submicrometer-scale particles. We show that controlled spatial variations in the liquid crystal's alignment convert the torque on a wire to a translational force that levitates the wire to a specified height.

Complex fluids are soft materials that have liquid-like properties but differ from ordinary liquids because of internal structure on the nanometer or micrometer scale. The classic example of a complex fluid is a polymer solution containing long chain-like molecules whose presence alters the flow behavior. Complex fluids are ubiquitous; they occur, for example, in living organisms and in many important technologies. When particles are suspended in a complex fluid, effects from entropy, interfacial phenomena, or other sources can generate forces on the particles that are not present in ordinary liquids (*1*). Understanding and controlling these forces are important scientific challenges. For example, the emergent technique of microrheology uses the motion of small particles in a complex fluid to uncover characteristics of the fluid at length scales and time scales that are inaccessible to bulk probes (*2*). The relations between the forces that give rise to this motion and the intrinsic properties of the fluid are key to interpreting microrheology experiments. Alternatively, the forces imposed on particles in a complex fluid can be used to manipulate the particles and arrange them into unique and useful structures (*3*–*6*).

Nematic liquid crystals are complex fluids possessing anisotropy that introduces both forces and torques on suspended particles (*7*–*17*). A nematic is composed of rod-like molecules and is characterized by an alignment of the long axes of the molecules along a particular direction. At an interface between a nematic and a surface, interactions between the surface and the liquid crystal molecules can create an energetically preferred orientation for the nematic alignment. For surfaces that are not flat, such as those of particles suspended in the nematic, these preferences can distort the otherwise uniform alignment, with a corresponding cost to the nematic's elastic energy. The tendency to minimize this energy can lead to forces on the particles. For example, recent studies on spherical particles that orient the nematic perpendicular to their surface have shown that the resulting distortions mediate interactions between the particles (*7*–*12*). However, few probes exist that can directly access such forces. Hence, despite their significance, few geometries exist for which quantitative information about them has been extracted (*8*, *12*, *18*), and the exploitation of these forces for manipulating particles remains largely unexplored. We have developed methods to manipulate anisotropic particles in nematic liquid crystals. The particles' shape introduces orientational degrees of freedom that lead to fluid-imposed forces and torques, which we have measured quantitatively. Specifically, by balancing the fluid-imposed forces on magnetic nanowires with either applied magnetic fields or gravity, we have determined the elastic torque on a wire and have measured a repulsion between a wire and a flat surface that is mediated by the nematic. As a demonstration of how these interactions can be controlled, we showed that a spatial variation in the nematic's alignment converts the torque into a translational force that can levitate a wire to a desired height.

In our experiments, isolated, highly cylindrical nickel wires 175 nm in radius (*19*) were contained in the room-temperature nematic liquid crystal pentylcyanobiphenol (5CB). The wire lengths ranged from 14 to 35 μm. The 5CB with nanowires was held between parallel glass plates, which were separated by 100 μm. The plates were coated with rubbed polyimide to create a uniform orientation for the nematic alignment parallel to the plates. Typically, one specifies the local alignment direction for a nematic by a

Department of Physics and Astronomy, Johns Hopkins University, Baltimore, MD 21218 USA.